

Integrated Performance and Critical Issues for Steady-State Operation in JT-60U

Yoshiteru SAKAMOTO and the JT-60 team

Japan Atomic Energy Agency, 801-1, Mukouyama, Naka, Ibaraki, 311-0193, Japan

(Received 19 January 2009 / Accepted 1 September 2009)

This paper reports on the integrated performance achieved in JT-60U toward the steady-state operation foreseen in the ITER and DEMO reactors. Advanced tokamak plasmas with weak shear or reversed shear have been optimized to confront critical issues such as high-beta operation with high confinement, the compatibility of high-density operation with high confinement, and long sustainment with a high non-inductive current drive fraction. As a result, high-integrated performance was achieved in both plasma regimes. For example, high-confinement reversed shear plasmas with a high bootstrap current fraction exceeding the no-wall beta limit have been obtained in the reactor relevant $q_{95} \sim 5.3$; high values of $\beta_N \sim 2.7$, $HH_{98y2} \sim 1.7$, $n_e/n_{GW} \sim 0.87$, and $f_{BS} \sim 0.9$ are simultaneously achieved with a reversed q profile with $q_{min} \sim 2.3$.

© 2010 The Japan Society of Plasma Science and Nuclear Fusion Research

Keywords: advanced tokamak, integrated performance, DEMO reactor, high beta, high density, high confinement, long sustainment

DOI: 10.1585/pfr.5.S1008

1. Introduction

High fusion performance has been achieved in JT-60U, one of the largest tokamaks in the world. For example, record values of fusion triple product $n\tau T = 1.53 \times 10^{21} \text{ m}^{-3} \text{ s keV}$ [1] and DT equivalent fusion gain $Q_{DT}^{eq} = 1.25$ have been achieved [2]. For steady-state operation of a tokamak, however, high integrated performance is required, involving long sustainment of high values of the confinement enhancement factor over ELMy H-mode scaling (HH_{98y2}), normalized beta (β_N), bootstrap current fraction of plasma current (f_{BS}), non-inductive driven current fraction of plasma current (f_{CD}), fuel purity, ratio of radiation loss power to absorbed heating power (f_{rad}), and normalized electron density versus Greenwald density limit (n_e/n_{GW}) [3]. For example, the ITER steady-state operation scenario predicts $HH_{98y2} = 1.61$, $\beta_N = 2.93$, $f_{BS} = 0.46$, $f_{CD} = 1.0$, a fuel purity of 0.82, $f_{rad} = 0.53$, and $n_e/n_{GW} = 0.78$ [4]. Furthermore, other reactor relevant conditions, such as the operation region of $q_{95} \sim 5$, an electron temperature nearly equal to the ion temperature, and a low momentum input due to alpha heating, are also important.

In JT-60U, two types of advanced tokamak plasmas, with an internal transport barrier (ITB) and with an edge transport barrier (ETB), have been optimized toward high-integrated performance [5]. One is a high β_p H-mode plasma, a so-called weak shear plasma, which is characterized by a safety factor (q) profile with weak positive magnetic shear in the core region, a parabolic-type weak ITB, and a higher beta limit than reversed shear plasmas. The other is a reversed shear H-mode plasma characterized

by a q profile with negative magnetic shear in the core region, a box-type strong ITB, and a larger bootstrap current fraction and higher confinement than weak shear plasmas.

This paper focuses on the following critical issues for high integrated performance. The first issue is simultaneous achievement of high beta and high confinement, because these features directly enhance fusion performance. Second is the compatibility of high density with high confinement. Since a large amount of particle fueling by gas puffs degrade the temperature in the core region, we should develop high-density operation while maintaining high confinement. Third is long sustainment, which requires demonstration of steady-state plasma with a high non-inductive current drive fraction over characteristic timescales, for example, the energy confinement time (τ_E) and current diffusion time (τ_R).

This paper describes the progress toward integrated performance in weak shear and reversed shear plasmas in JT-60U and is organized as follows. High-beta operation above the no-wall beta limit is described in section 2. High-density operation with high confinement is described in section 3. Long sustainment with a high non-inductive current drive fraction is described in section 4. A summary is presented in section 5.

2. High Beta Operation above the No-Wall Beta Limit

High-beta operation is approached by optimizing the current and pressure profiles and the magnetic configuration. For example, a peaked current profile, a broad pressure profile, and a high-triangularity configuration are effective for achieving higher beta, although a broader cur-

author's e-mail: sakamoto.yoshiteru@jaea.go.jp

rent profile is expected in the DEMO reactor due to high f_{BS} . The stability limit of ideal low- n kink modes is significantly improved when a plasma is close to a perfectly conducting wall. However, resistive wall modes (RWMs), which are a branch of ideal low- n kink modes, are destabilized due to the finite resistivity of the conducting wall when the plasmas exceed the no-wall beta limit due to the ideal low- n kink modes. RWM stabilization has been demonstrated by using an externally applied non-axisymmetric magnetic field with coils [6] and/or by sufficient plasma rotation [7]. Furthermore, recent study of spontaneous rotation suggests that spontaneous rotation in ITER is high enough to stabilize RWMs without external momentum input [8]. Therefore, both methods would be applicable to future devices. Recent experiments in JT-60U and DIII-D demonstrated a low toroidal rotation threshold for stabilizing RWMs, where the toroidal rotation velocity at the low-order rational surface plays an important role [9, 10]. Recently, the installation of ferritic steel tiles in JT-60U enabled us to produce a large-volume plasma configuration close to the conductive wall for wall stabilization, with high heating power due to the reduction of fast ion losses by toroidal field ripples.

In the weak shear plasma regime, high β_N (~ 4) was transiently achieved by wall stabilization [11]. In such high- β_N plasmas, toroidal rotation becomes slower due to the large fast ion loss caused by high-powered injection of perpendicular neutral beams (NBs), which makes long sustainment difficult. Recently, a stationary weak shear plasma with wall stabilization was obtained by controlling the toroidal rotation velocity to keep it above the critical velocity [12].

Figure 1 shows the waveform of the stationary sustained weak shear plasma above the no-wall beta limit,

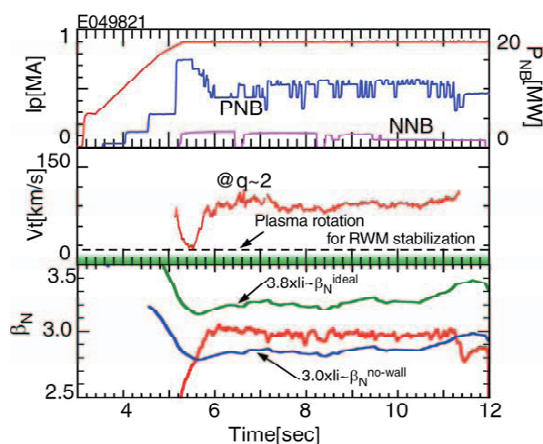


Fig. 1 Waveforms of stationary sustained weak shear plasma with wall stabilization. (a) Plasma current and injected heating power. (b) Toroidal rotation velocity at $q \sim 2$ surface together with critical velocity level for RWM stabilization. (c) Normalized beta together with no-wall beta limit and ideal-wall beta limit.

where $\beta_N \sim 3$ was sustained for ~ 5 s. Here, the plasma current $I_p = 0.9$ MA, the toroidal magnetic field $B_T = 1.44$ T, $q_{95} \sim 3.3$, and the ratio of the wall radius to the plasma minor radius $d/a \sim 1.3$. In the discharge, low-power NB heating was applied during the I_p ramp-up phase to produce the weak positive shear configuration, and high-power NB heating with a negative-ion-based neutral beam (N-NB) was injected to produce an ITB. β_N was sustained by using feedback control of stored energy via perpendicular NBs. The toroidal rotation velocity at the $q \sim 2$ surface was much faster than the critical velocity, ~ 20 km/s, as shown in the figure. The no-wall beta limit is roughly indicated as 3.0 times the internal inductance, while the ideal-wall beta limit is 3.8 times the internal inductance, which is confirmed by the MARG2D code [13]. According to the ACCOME code [14], which solves the inductive and non-inductive current density profiles consistent with plasma equilibrium, $f_{CD} > 0.8$ and $f_{BS} \sim 0.5$ were achieved. Since a large-volume configuration was utilized for wall stabilization, the lower confinement ($HH_{98y2} \sim 0.8$) is attributed to the lack of strong central heating. The duration of sustainment above the no-wall beta limit is determined by the increase in the no-wall beta limit due to gradual penetration of the inductive field. β_N decreased at $t \sim 11.2$ s not because of magnetohydrodynamic (MHD) activities but because of a decrease in the injected power due to the interlock in the NB system. Furthermore, some MHD instabilities cause disruption in high-beta weak shear plasmas above the no-wall beta limit. In particular, the $n = 1$ bursting mode and slowly growing mode have been observed as RWM precursors [12]. The bursting mode, the so-called energetic-particle-driven wall mode (EWM) [15], is the energetic particle branch resulting from the interaction between the energetic particle and a marginally stable RWM, and directly triggers the RWM despite the presence of enough toroidal rotation velocity for RWM stabilization. The slowly growing mode, whose growth time is longer than the resistive wall time, reduces the toroidal rotation velocity and its shear at the rational surface, followed by the destabilization of the RWM.

Since the attainable beta limit is typically $\beta_N \sim 2$ in JT-60U reversed shear plasmas with $d/a > 1.5$ (without wall stabilization), one of the most critical issues is the enhancement of β_N for the DEMO reactor [16]. Typical waveforms of the discharge above the no-wall beta limit in the reversed shear plasma regime are shown in Fig. 2, where the plasma parameters are $I_p = 0.8$ MA, $B_T = 2.0$ T, $q_{95} \sim 5.3$, and $d/a \sim 1.3$ [16]. The value of q_{95} is close to the design parameter of the DEMO reactors. The discharge was established under the low-momentum input condition expected in DEMO reactors, where tangential NBs were injected in a balanced way in which the injected power of co-tangential NBs is similar to that of ctr-tangential NBs. The normalized beta increased continuously following stored energy feedback control. However, the discharge was terminated by disruption at $t \sim 6.1$ s. MHD in-

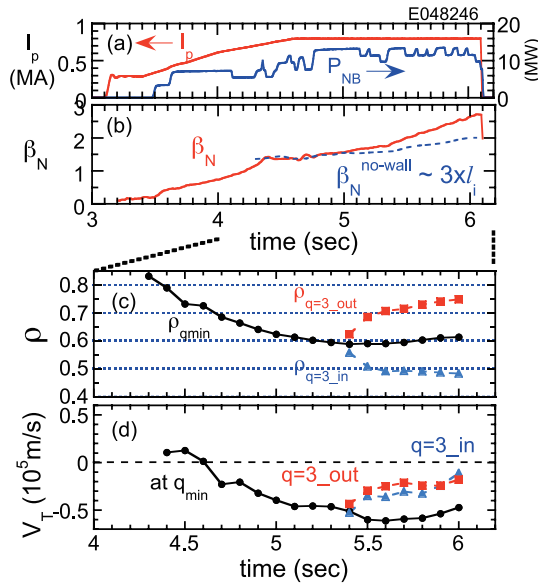


Fig. 2 Waveforms of wall-stabilized reversed shear discharge. (a) Plasma current and injected heating power. (b) Normalized beta together with no-wall beta limit. (c) Normalized minor radius of q_{\min} and $q = 3$ surfaces. (d) Toroidal rotation velocities at q_{\min} and $q = 3$ surfaces.

stability ($n = 1$) was observed just before the disruption, of which the growth time is on the order of the resistive wall time ($\tau_W \sim 10$ ms), suggesting the RWM. In this discharge, $\beta_N \sim 2.7$ was achieved just before disruption, and the achieved high β_p (~ 2.3) leads to high f_{BS} . The achieved value of β_N is much higher than that of reversed shear plasmas with $\beta_N \sim 1.7$ – 2.2 at $d/a \sim 1.5$. The no-wall beta limit is estimated at about three times the internal inductance, as shown in the figure. Detailed analysis of MHD stability using the MARG2D code indicates that the ideal wall beta limit is $\beta_N \sim 2.9$, and the no-wall beta limit is ~ 1.9 , resulting in $C_\beta \sim 0.8$, where $C_\beta = (\beta_N - \beta_N^{\text{no-wall}}) / (\beta_N^{\text{ideal-wall}} - \beta_N^{\text{no-wall}})$.

Note that values of q such as $q_{95} \sim 5.3$, $q_{\min} \sim 2.3$, and $q(0) \sim 10$ are very similar to those of ITER steady-state scenario (VI) for strong negative shear, in which $q_{95} \sim 5.4$, $q_{\min} \sim 2.3$, and $q(0) \sim 5.9$ are expected [4]. Thanks to strong ITBs, at which thermal diffusivities decrease to the level of neoclassical transport for ions, a high confinement enhancement factor $HH_{98y2} \sim 1.7$ was obtained at high normalized density ($n_e/n_{GW} \sim 0.87$), and the ratio of electron and ion temperatures (T_e/T_i) was ~ 0.9 at the center. Furthermore, an extremely high bootstrap current fraction of $\sim 92\%$, which is evaluated from the ACCOME code, is obtained in the plasma. The RWM became unstable when toroidal rotation velocities at the $q = 3$ surface decreased to the critical toroidal rotation velocity, as shown in Fig. 2 (d). Comparison of the balanced and co-injected discharges might reveal that the toroidal rotation velocity at the outer $q = 3$ surface plays an important role in RWM stabilization [16]. The improvement factor of β_N with/without the

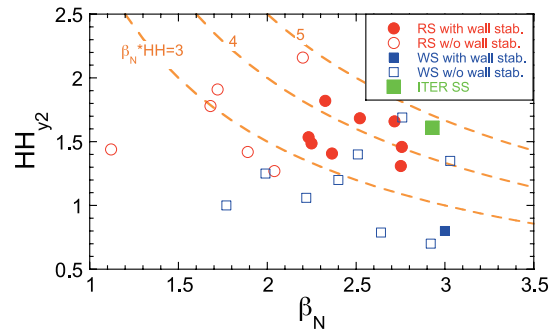


Fig. 3 Simultaneous achievement of high normalized beta and high confinement. Red and blue symbols indicate reversed shear and weak shear plasmas, respectively, and open and closed symbols indicate the presence and absence of wall stabilization, respectively. Green squares mark the ITER steady-state operation scenario. Dotted curves correspond to the products of normalized beta and confinement enhancement factor.

conductive wall is ~ 1.5 in plasma with the reversed shear configuration. The improvement factor is higher than that in the plasma with positive shear configuration, which is typically ~ 1.3 [9]. The reason for the difference might be that the off-axis current, which is one of the driving terms of the ideal kink-ballooning mode, is larger in a reversed shear plasma than in a positive shear plasma, which leads to a difference in eigen-function of the mode near the plasma surface.

Figure 3 shows the simultaneous achievement of high beta and high confinement in both weak shear and reversed shear plasmas with/without wall stabilization. The beta limit was improved by RWM stabilization, especially in reversed shear plasmas, while maintaining high confinement. A high value of β_N (~ 3) was achieved with a high HH_{98y2} (~ 1.5) in both plasma regimes, which is expected in the ITER steady-state operation scenario. In weak shear plasmas, high β_N and high confinement were obtained even without wall stabilization, as shown in the figure, where the more peaked current profile leads to a higher no-wall beta limit. On the other hand, lower confinement in the weak shear plasma with wall stabilization is attributed to the lack of strong central heating.

3. High-Density Operation with High Confinement

Although high-density operation above the Greenwald density is preferable in the DEMO reactors, confinement degradation was observed in ELMy H-mode plasmas without ITBs [17]. In plasmas with an ITB, strong central heating is required to sustain high confinement, especially in weak shear plasmas. However, it is difficult to keep a centrally peaked heating profile at high density due to attenuation of NB as particle fueling. Multiple pellet injection has enabled us to widen the particle control capability.

Figure 4 compares high-density operation in weak shear plasma discharge with pellet injection and with gas fueling [18], where the electron density was enhanced up to $n_e/n_{GW} \sim 0.7$, with $B_T = 3.6$ T, $I_p = 1.0$ MA, $q_{95} \sim 6.5$, and $\delta \sim 0.45$. Pellets were injected from the high field side. In addition, an N-NB, which has a high beam energy (~ 360 keV), was injected at the high-density phase to maintain a centrally peaked heating profile. In pellet-injected discharge, the confinement enhancement factor over L-mode scaling (H_{89PL}) stayed almost constant even with increasing electron density, as shown in Fig. 4 (a), where $HH_{98y2} = 1.05$, $\beta_N = 2.2$, and $f_{BS} \sim 60\%$ were simultaneously achieved at $n_e/n_{GW} \sim 0.7$. On the other hand, H_{89PL} decreases with increasing electron density in gas-fueled discharge, as shown in Fig. 4 (b). The ITBs in the temperature profile were sustained and the density profile was peaked in the pellet-injected discharge, while the ITBs produced in the early phase disappeared in the gas-fueled discharge. One of the differences is seen in the pedestal parameter. The electron density at the pedestal is almost the same in both discharges, while the temperatures at the pedestal are higher in the pellet-injected discharge than in the gas-fueled discharge. The pedestal temperature and density increase gradually with time in the pellet-injected discharge, where core-edge parameter linkage plays an important role [18]. On the other hand, the temperature decreases with increasing density in the gas-fueled discharge,

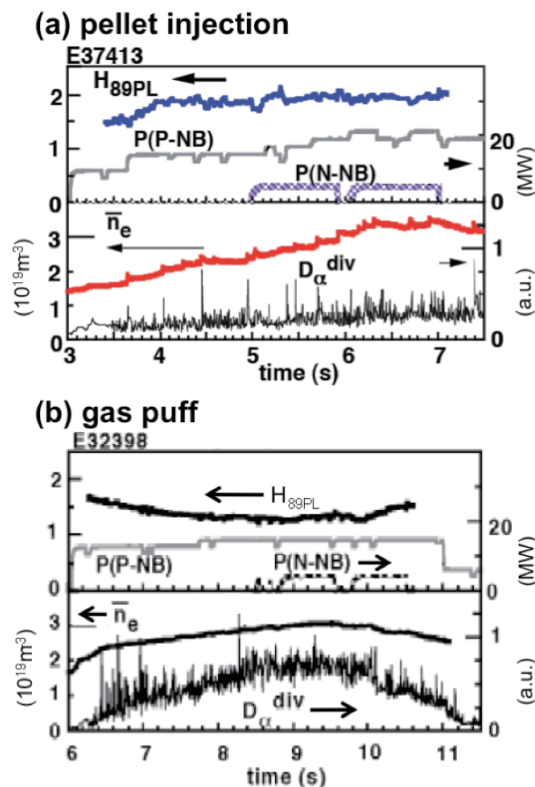


Fig. 4 Waveforms of high-density operation utilizing (a) pellet injection and (b) gas puffs.

which leads to a decrease in the core temperature and energy confinement.

In the reversed shear plasma regime, on the other hand, stronger ITBs are produced, including the electron density profile. The wide ITB radius can contribute to maintaining high confinement characteristics during high-density operation. Figure 5 shows the electron density profile normalized to the Greenwald density in high-density reversed shear plasma before ITB formation and at the fully developed ITB phase [19]. Here, $B_T = 2.5$ T, $I_p \sim 1.0$ MA, and $q_{95} \sim 6.1$, and NB and lower hybrid range of frequencies (LHRF) heating were utilized. Note that the density increases only with NB fueling. The density profile changes from relatively flat to a broad central-peaked profile, where the density inside the ITB increases while the edge density remains almost constant. Although the edge electron density is smaller than $0.4n_{GW}$, the central electron density largely exceeds n_{GW} due to the wide radius of the ITB. Therefore, a high n_e/n_{GW} is obtained due to the peaked density profile inside the wide ITB. Because of the ITBs, $HH_{98y2} = 1.3$, $\beta_N \sim 2$, and $f_{BS} \sim 70\%$ were simultaneously achieved at $n_e/n_{GW} = 1.1$. The pedestal pressure is lower than that in ELMy H-mode plasmas, and the core-edge parameter linkage is weak compared to that in weak shear plasmas.

Figure 6 shows the compatibility of high density and high confinement in both weak shear and reversed shear plasmas; standard ELMy H-mode and impurity-seeded plasmas [19] are also shown. Confinement performance is degraded with increasing n_e/n_{GW} in ELMy H-mode, weak shear, and reversed shear plasmas. The high-density operation region is expanded in weak shear plasmas with small degradation of the confinement property by using density profile control (for example, by pellet injection as described above) and impurity seeding with argon. A high confinement region of $HH_{98y2} (> \sim 1)$ was achieved up to $n_e/n_{GW} \sim 0.9$. Furthermore, a high-density operation region at $n_e/n_{GW} \sim 1$, foreseen in the ITER steady-state

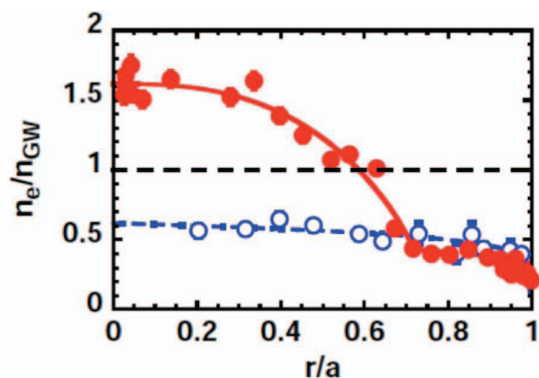


Fig. 5 Profiles of electron density normalized by Greenwald density obtained in high-density reversed shear plasma before ITB formation (open circles) and at the fully developed ITB phase (closed circles).

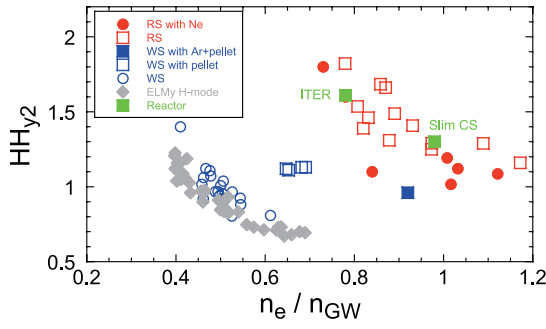


Fig. 6 Compatibility of high density and high confinement in weak shear and reversed shear plasmas together with ELMy H-mode (closed diamonds). Red and blue symbols indicate reversed shear and weak shear plasmas, respectively, and closed and open symbols indicate the presence and absence of impurity seeding, respectively. Green symbols mark the ITER steady-state operation scenario and Slim CS. Open squares indicate weak shear plasmas with pellet injection.

operation scenario and DEMO reactors such as the Slim CS, was obtained in reversed shear plasmas with a very high confinement property ($HH_{98y2} = 1.3-1.7$). In addition to high-density operation, a high radiation loss fraction ($f_{rad} > 0.9$) was also obtained in the cases of impurity-seeded discharge. $HH_{98y2} \sim 0.95$ at $n_e/n_{GW} \sim 0.7$ has been obtained so far under the wall-saturated condition, which is expected in steady-state plasmas [20].

4. Long Sustainment with High Non-Inductive Current Drive Fraction

The long sustainment of plasmas with full non-inductive current drive is required for steady-state tokamak operation. A critical issue for long sustainment is avoidance of neoclassical tearing modes (NTMs) for weak shear plasmas and avoidance of disruption in reversed shear plasmas.

In the weak shear plasma regime, suppression of NTMs was demonstrated by electron cyclotron current drive [21]. However, for complete avoidance of the NTM with $m/n = 3/2$, the value of q in the whole plasma region must be greater than 1.5. In addition, it is preferable that the location of $q = 2$ shifts strongly outwards, making the pressure gradient small enough for the mode to occur, thanks to the large bootstrap current driven at the off-axis region. A typical waveform of such a scenario is shown in Fig. 7 [22], where $I_p = 1$ MA, $B_T = 2.4$ T, $\kappa = 1.44$, $\delta = 0.5$, and $q_{95} \sim 4.5$. A plasma with $\beta_N \sim 2.4$ ($\beta_p \sim 1.7$) has been sustained for 5.8 s. This duration corresponds to $\sim 26\tau_E$ and $\sim 2.8\tau_R$. The loop voltage was reduced to nearly zero, indicating nearly full non-inductive current drive. Analysis of the non-inductive current drive indicates that $f_{BS} \sim 43-50\%$ and $f_{BD} \sim 47-52\%$ were obtained. The duration of sustainment was determined by the pulse length of N-NB (~ 4 MW, ~ 6.5 s). In this discharge, $HH_{98y2} \sim 1.0$ was

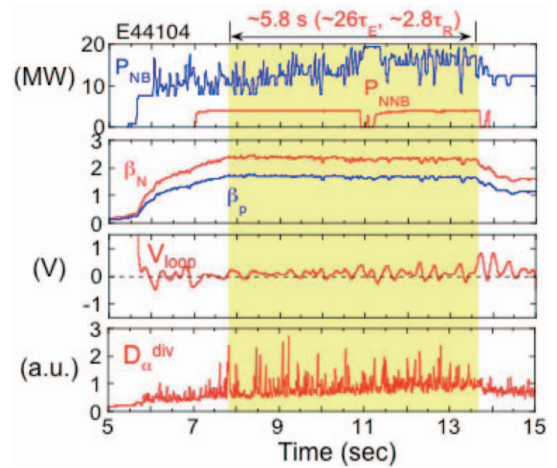


Fig. 7 Waveforms of long-sustained weak shear plasma with nearly full non-inductive current drive.

obtained at $n_e/n_{GW} \sim 0.54$. It should be emphasized that no NTM due to the optimization of the q profile was observed in this discharge. Pressure and q profiles were optimized by feedback control of stored energy and injection timing of NBs. The NB was injected at $t \sim 5.6$ s, before full penetration of the inductive current; the shape of the q profile at $t = 5.6$ s is monotonic, and $q > 1.5$ in the whole plasma region. During the initial phase of NB heating ($t = 5.6-7.0$ s), β_N was carefully raised to ~ 2.0 by feedback control of stored energy to avoid NTM destabilization. In this low- β_N phase, the q profile was flattened, the $q = 2$ surface moved outward, and $q > 1.5$ in the whole plasma region due to the increase in bootstrap current around the off-axis region. The q profile in the core region became slightly reversed at $t = 7.0$ s. After the q profile flattened, an N-NB was injected to enhance the non-inductive current drive and increase β_N from ~ 2.0 to ~ 2.4 . In the later phase of the discharge, the q profile was similar to that at an earlier time but slightly decreased. The minimum value of q was kept $> \sim 1.5$, and the $q = 2$ surface was located in the small temperature gradient region; then, no NTM was observed.

In the reversed shear plasma regime, one of the difficulties in obtaining long sustainment is avoiding disruption due to the lower beta limit without wall stabilization. The reversed shear q profile gradually changes toward the stationary condition, where the value of q in the core plasma region, including q_{min} and its location, decreases continuously due to penetration of the inductive field. Therefore, the value of q_{min} passes through integer values until reaching the stationary condition. Then, discharges are frequently terminated by disruption when q_{min} goes across the integer values. To avoid disruption, the pressure gradient at the ITB should be decreased when the plasma becomes unstable.

A technique for controlling the ITB strength was developed in JT-60U reversed shear discharges by controlling toroidal rotation, as local reduction of the E_r shear af-

fects the whole ITB layer [23]. For long sustainment of reversed shear plasmas with large f_{BS} under nearly full non-inductive current drive, we attempted toroidal rotation control to avoid disruption. Typical waveforms of the long-sustained reversed shear discharge are shown in Fig. 8; $I_p = 0.8$ MA, $B_T = 3.4$ T, $q_{95} \sim 8.3$, $\kappa_x = 1.6$, and $\delta_x = 0.42$ [22]. Utilizing feedback control of the stored energy by perpendicular NBs, $\beta_N \sim 1.7$ ($\beta_p \sim 2.4$) was maintained from $t \sim 5.1$ s until the end of NB heating ($t = 12.5$ s). The loop voltage decreased to nearly zero and was kept nearly constant, indicating nearly full non-inductive current drive. A high HH_{98y2} of ~ 1.9 was also maintained due to ITBs at $n_e/n_{GW} \sim 0.6$. According to the ACCOME code, $f_{CD} > 0.9$ and $f_{BS} \sim 0.75$ were achieved. In this discharge, toroidal rotation control for pressure gradient control was applied during $t = 7-8$ s at $q_{min} = 4$, when the counter-NB was switched off; disruption was successfully avoided. The sustained duration of $f_{BS} \sim 0.75$ is ~ 7.4 s, which corresponds to $\sim 16\tau_E$ and $\sim 2.7\tau_R$. At the stationary phase, the profile of measured total current density agrees closely with that of non-inductive current density, which implies that the plasma approached the stationary condition.

Figure 9 shows the progress in long sustainment of

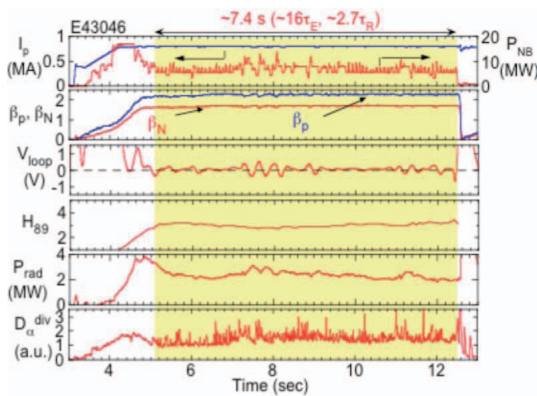


Fig. 8 Waveforms of long-sustained reversed shear plasma with nearly full non-inductive current drive.

weak shear and reversed shear plasmas with high f_{BS} . By optimizing the current and pressure profiles, the sustained duration of both plasma regimes is extended under the nearly full non-inductive current drive. The plasmas with high f_{BS} expected in the ITER steady state scenario and DEMO reactor are sustained for longer than the current diffusion time scale, which is typically ~ 2 s in JT-60U. Durations are limited by the pulse length of the NB or N-NB.

5. Summary

The JT-60U tokamak optimized weak shear and reversed shear plasmas toward steady-state operation of the tokamak and demonstrated (1) simultaneous high beta and high confinement, (2) compatibility of high density with high confinement, and (3) long sustainment under nearly full non-inductive current drive. As a result, high integrated performance was achieved in both plasma regimes. The integrated performance achieved in weak shear and reversed shear plasmas is shown in Figs. 10 (a) and 10 (b) together with the design parameters of the ITER steady-state scenario [4]. In the weak shear plasma regime, the discharge with high confinement and high beta plasma under full non-inductive current drive [3] and the discharge with high density produced by pellet injection are shown in the figure. In the reversed shear plasma regime, the discharge with high confinement and high beta plasma at reactor rel-

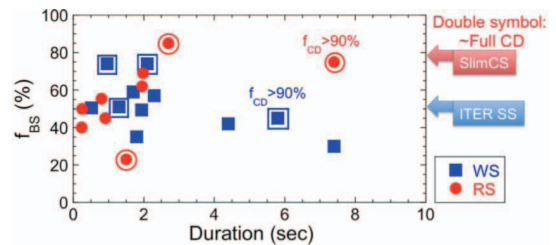


Fig. 9 Progress in long sustainment of high bootstrap current fraction plasmas. Red and blue symbols indicate reversed shear and weak shear plasmas, respectively, and double symbols indicate nearly full non-inductive current drive.

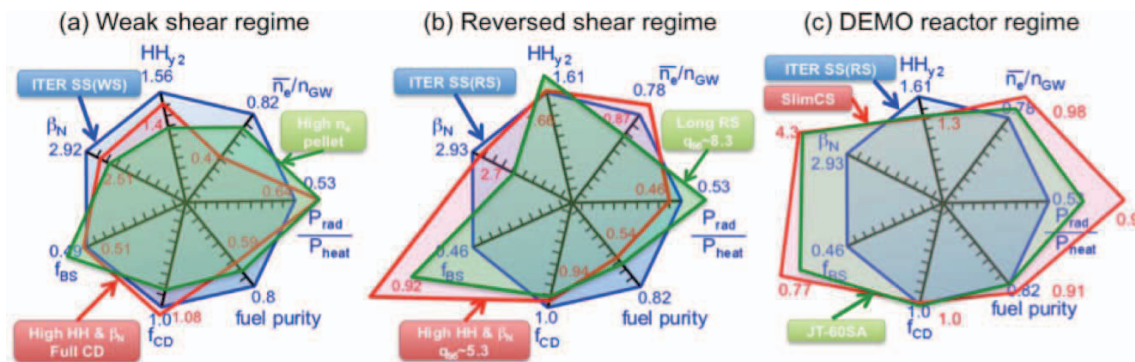


Fig. 10 Integrated performance achieved in (a) weak shear plasmas and (b) reversed shear plasmas. The full scale for each axis represents the design parameters of the ITER steady-state operation scenario. (c) Comparison of integrated performance of ITER, Slim CS, and JT-60SA.

evant $q_{95} \sim 5.3$ and the long pulse discharge at high $q_{95} \sim 8.3$ are shown in the figure. In both plasma regimes, high integrated performance compared to the ITER steady-state scenario was achieved. However, some parameters were not satisfied simultaneously. Also, long sustainment with high beta remains a concern.

Concerning the DEMO reactors, Slim CS [24] is an example of a compact DEMO reactor with high β_N (~ 4.3) and high f_{BS} (~ 0.77). Figure 10(c) compares the integrated performance of the ITER steady state scenario, Slim CS, and JT-60SA [25]. There are large gaps between the design parameters of Slim CS and ITER, especially in β_N , f_{BS} , and f_{rad} . JT-60SA will address these critical issues for DEMO, as a satellite tokamak of ITER, where high-beta operation will be demonstrated by RWM control coils, and heat and particle control will be performed with a strong divertor pumping capability. Thus, we hope the ITER scenario can be improved by the results of JT-60SA.

Acknowledgments

The authors acknowledge the members of the Japan Atomic Energy Agency who have contributed to the JT-60U projects.

- [1] S. Ishida *et al.*, Proc. 16th Int. Conf. Plasma Physics and Controlled Nuclear Fusion Research, Montreal, Canada, October 7-11, 1996, Vol. 1, p. 315, International Atomic Energy Agency (1997).
- [2] T. Fujita *et al.*, Nucl. Fusion **39**, 1627 (1999).
- [3] Y. Kamada and the JT-60 team, Nucl. Fusion **41**, 1311 (2001).
- [4] Plasma Performance Assessment 2004 section 3.4, ITER Technical Basis ITER EDA Documentation Series.
- [5] Y. Kamada *et al.*, Fusion Sci. Technol. **42**, 185 (2002).
- [6] C.M. Bishop, Plasma Phys. Control. Fusion **31**, 1179 (1989).
- [7] A. Bondeson and D.J. Ward, Phys. Rev. Lett. **72**, 2709 (1994).
- [8] J.E. Rice *et al.*, Nucl. Fusion **47**, 1618 (2007).
- [9] M. Takechi *et al.*, Phys. Rev. Lett. **98**, 055002 (2007).
- [10] H. Reimerdes *et al.*, Phys. Rev. Lett. **98**, 055001 (2007).
- [11] M. Takechi *et al.*, Proc. 21st Int. Conf. on Fusion Energy (Chengdu, 2006) (Vienna: IAEA) EX/7-1Rb.
- [12] G. Matsunaga *et al.*, Proc. 22nd Int. Conf. on Fusion Energy (Geneva, 2008) (Vienna: IAEA) EX/5-2.
- [13] S. Tokuda and T. Watanabe, Phys. Plasmas **6**, 3012 (1999).
- [14] K. Tani *et al.*, J. Comput. Phys. **98**, 332 (1992).
- [15] G. Matsunaga *et al.*, Phys. Rev. Lett. **103**, 045001 (2009).
- [16] Y. Sakamoto *et al.*, Nucl. Fusion **49**, 095017 (2009).
- [17] H. Urano *et al.*, Plasma Phys. Control. Fusion **44**, 11 (2002).
- [18] Y. Kamada *et al.*, Plasma Phys. Control. Fusion **44**, A279 (2002).
- [19] H. Takenaga *et al.*, Nucl. Fusion **45**, 1618 (2005).
- [20] N. Asakura *et al.*, Nucl. Fusion **49**, 115010 (2009).
- [21] A. Isayama *et al.*, Nucl. Fusion **43**, 1272 (2003).
- [22] Y. Sakamoto *et al.*, Nucl. Fusion **45**, 574 (2005).
- [23] Y. Sakamoto *et al.*, Nucl. Fusion **41**, 865 (2001).
- [24] K. Tobita *et al.*, Nucl. Fusion **47**, 892 (2007).
- [25] T. Fujita *et al.*, Nucl. Fusion **47**, 1512 (2007).